tvst

Retina

# Inter-Individual Topographic Variation of Choroidal Thickness in Healthy Eyes on Swept-Source Optical Coherence Tomography

**Zehua Jiang[1,2], Tian Lin[1,2], Aidi Lin[1,2], Xujia Liu[1,2], Xiaoting Mai[1,2], Jianwei Lin[1], Carol Y. L. Cheung[3], and Haoyu Chen[1,2]**

[1] Joint Shantou International Eye Center of Shantou University and The Chinese University of Hong Kong, Shantou, China
[2] Medical College, Shantou University, Shantou, China
[3] Department of Ophthalmology and Visual Sciences, The Chinese University of Hong Kong, Shatin, Hong Kong

**Correspondence:** Haoyu Chen, Joint Shantou International Eye Center of Shantou University and The Chinese University of Hong Kong, Dongxia North Road, Shantou 515041, China.
e-mail: drchenhaoyu@gmail.com

**Received:** November 7, 2023
**Accepted:** February 27, 2024
**Published:** April 17, 2024

**Keywords:** choroidal thickness; swept-source optical coherence tomography; inter-individual variation; coefficient of determination

**Citation:** Jiang Z, Lin T, Lin A, Liu X, Mai X, Lin J, Cheung CYL, Chen H. Inter-individual topographic variation of choroidal thickness in healthy eyes on swept-source optical coherence tomography. Transl Vis Sci Technol. 2024;13(4):24, https://doi.org/10.1167/tvst.13.4.24

**Purpose:** To investigate the topographic characters of inter-individual variations of the macular choroidal thickness (CT).

**Methods:** This was a retrospective study. Macular CT data for 900 0.2 × 0.2-mm grids from 410 healthy eyes were collected from swept-source optical coherence tomography. Following the analysis of factors associated with mean CT, the $\beta$-coefficients of the included associated factors in each grid were summarized for choroidal thickness changes analysis. Additionally, the coefficient of variance (CoV), coefficient of determination (CoD), and coefficient of variance unexplained (CoVU) for CT were calculated in each individual grid to investigate the inter-individual choroidal variations pattern.

**Results:** Sex ($\beta = -17.26$, female vs. male), age ($\beta = -1.61$, per 1 year), and axial length ($\beta = -18.62$, per 1 mm) were associated with mean macular CT. Females had a thinner choroid in all 900 grids (0.5–26.9 µm). As age increased, the CT noticeably decreased (8.74–19.87 µm per 10 years) in the temporal regions. With axial length elongation, the thinning (7.94–24.91 µm per 1 mm) was more evident in subfoveal and nasal regions. Both the CoV (34.69%–58.00%) and CoVU (23.05%–40.78%) were lower in the temporal regions, whereas the CoD (18.41%–39.66%) was higher in the temporal regions.

**Conclusions:** Choroidal thinning is more predominant in the subfoveal and nasal regions with axial length elongation, but in the temporal region with aging. The inter-individual variation of CT is higher and less determined by sex, age, or axial length in the nasal regions.

**Translational Relevance:** Topographic variation should be considered when interpreting choroidal thickness.

## Introduction

The choroid, a vascular structure ranging from Bruch's membrane to the choroidal–scleral interface, plays an important role in supporting the structure and function of the retina.[1] The development of enhanced depth imaging[2] and swept-source optical coherence tomography (SS-OCT)[3] makes it possible for in vivo choroidal structure visualization and accurate thickness measurement. Previous studies have reported that changes in choroidal thickness (CT) are associated with physiological processes such as aging,[4] axial length elongation,[5] and the development of various eye diseases,[6] including age-related macular degeneration,[7] myopia,[8] and pachychoroid diseases.[9]

However, most of these studies focused only on the mean and subfoveal CT[10] or, in the case of the Early Treatment Diabetic Retinopathy Study (ETDRS), regional CT.[11,12] Indeed, the choroid is a three-dimensional structure, and the distribution of CT in healthy eyes remains inconclusive.[13] In widefield monitoring of the choroidal thickness and

vascular densities, the thickness values, symmetrical/asymmetrical patterns, and topography of the choroid are diverse.[14–16] Various studies have reported that the thickest areas are the superior,[17] temporal,[8,18] and subfoveal regions.[19] Also, studies have reported varied choroidal thickness distribution patterns,[14] suggesting the inter-individual CT variations are too complex to be evaluated based on several subregions.

Recently, a 900-grid analysis algorithm for CT has been developed for Triton Multimodal SS-OCT (Topcon Healthcare, Tokyo, Japan), allowing for nuanced evaluation of the topographic features of macular CT.[20,21] In this study, we investigated the relationship between CT in each of the 900 grids and various CT-associated factors to map CT variations. Additionally, we constructed distributions for the coefficient of variance (CoV), coefficient of determination (CoD), and coefficient of variance unexplained (CoVU) across the 900 grids. Incorporating all of these parameters resulted in comprehensive representations of the nuanced topographic patterns of inter-individual choroidal variation.

# Methods

## Data Collection

Our research adhered to the tenets of the Declaration of Helsinki. Institutional Review Board (IRB) approval was obtained from the Joint Shantou International Eye Center (JSIEC) of Shantou University and The Chinese University of Hong Kong. Informed consent was not required by the IRB as this was a retrospective study.

Outpatient records with OCT examinations from January 2018 to November 2020 at JSIEC were reviewed to identify healthy individuals with no systemic diseases. OCT images with a resolution of 512 $\times$ 256 pixels were obtained from the Triton Multimodal SS-OCT using a three-dimensional 7 $\times$ 7-mm macular scanning mode. Patients with chorioretinal diseases, glaucoma, history of ocular surgery or treatment, or OCT image quality scores below 40 were excluded. Also, given the interocular symmetry pattern,[22,23] only one eye of each included individual was enrolled randomly for analysis.

For every included eye, segmentation of the choroid (from Bruch's membrane to the choroidal–scleral junction) in each B-scan image was manually checked by a trained clinician who was masked to the subjects' clinical information to rectify any potential segmentation errors. Axial length and refractive error were input to correct magnification errors using the inbuilt algorithm of the Triton Multimodal SS-OCT.[24] Finally, CT data for 900 0.2 $\times$ 0.2-mm grids in the 6 $\times$ 6-mm macular areas were collected.

Also included for further correlation analysis were general information regarding sex and age; basic ophthalmic parameters of uncorrected visual acuity on a logMAR scale; diopter spherical and cylindrical refraction; axis of astigmatism; and spherical equivalents obtained from a Topcon full automatic optometer (KP8800). Other data collected included intraocular pressure (Haag-Streit AG, Köniz, Switzerland) and biological parameters including axial length, anterior chamber depth, lens thickness, and central corneal thickness obtained from ocular biometry (OA-2000; Tomey Corporation, Nagoya, Japan).

## Study Design

Figure 1 shows a flowchart of the study protocol and data analysis. First, the association of all demographic and clinical parameters with the mean CT in the whole macular region was analyzed by univariable regression. The parameters with $P < 0.05$ in univariable regression were then subjected to multivariable regression analysis for the mean macular CT. Statistically significant variants of all parameters from the multivariable regression were included in the further analysis of each grid. Then, each 0.2 $\times$ 0.2-mm grid was regarded as an independent area in the following data analysis.

The associated factors identified in the previous step were included in multivariable regression analyses to observe their relationship of the CT in each grid ($y_1 \sim y_{900}$) by R Studio 4.1.3 (R Foundation for Statistical Computing, Vienna, Austria). The $\beta$-coefficients of each factor were collected to analyze changes in the thickness of the choroid for every 1 unit of change in the corresponding factor for each grid.

The inter-individual variation of CT was evaluated using our self-defined CoV, CoD, and CoVU. The CoV, calculated as the ratio of the CT standard deviation to its mean thickness value in the 410 eyes, was used to describe the inter-individual variation in each grid. The CoD, the $R^2$ values of the associated factors from multivariable regression, was collected to evaluate the extent to which each associated factor accounted for the inter-individual variation within each grid. The CoVU values were computed as CoV $\times$ (1 – CoD) to determine the residual inter-individual variations that remained unexplained by the associated factors.

Finally, the $\beta$-coefficients of the 900 grids for each associated factor (CoV, CoD, and CoVU)

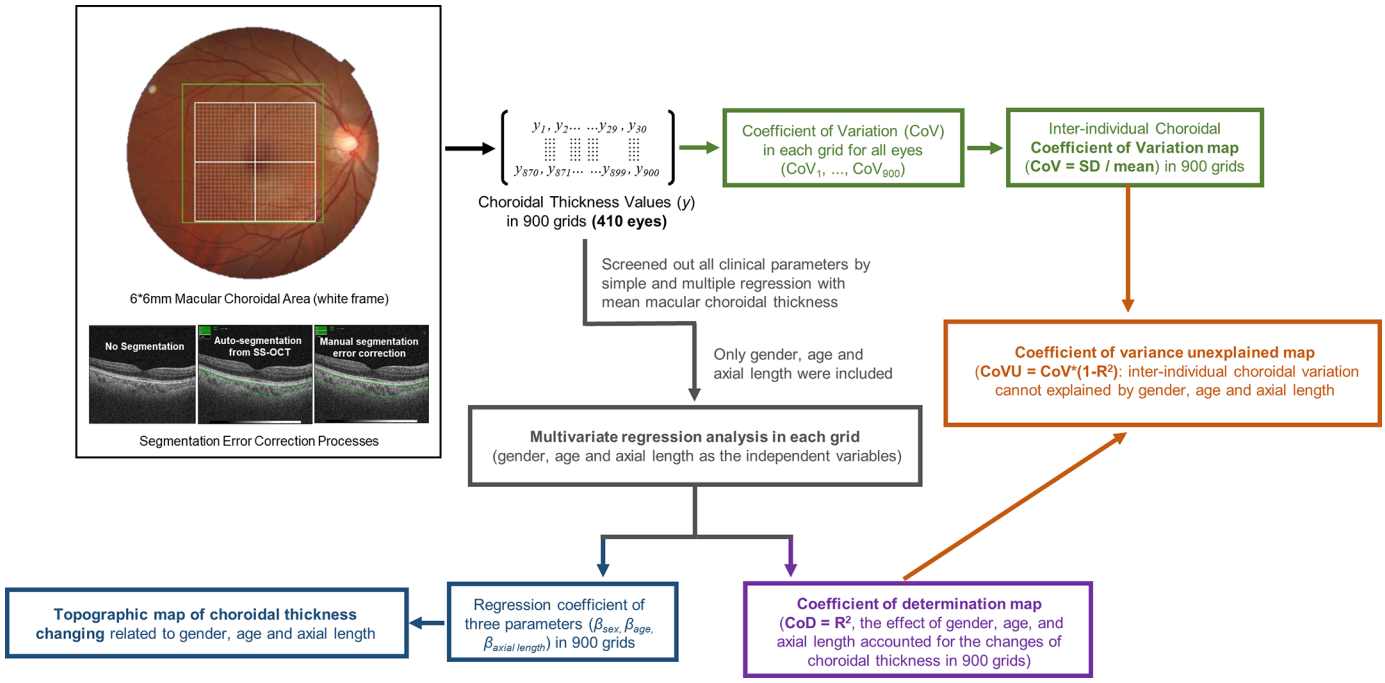


**Figure 1.** Flowchart of the study protocol.

were summarized as topographic maps constructed using Excel (Microsoft Corporation, Redmond, WA). For better visualization, left-to-right reversal was performed in all left-eye samples, aligning the temporal-to-nasal direction with the left-to-right.

# Results

## General Information and Screening of Influence Factors

A total of 410 samples were collected, encompassing individuals 6 to 87 years old (mean age, 33.59 ± 25.21 years), including 198 males (48.29%) and 212 females (51.71%), and the mean CT of the whole macular area was 195.20 ± 70.53 µm (Table). The mean macular CT was found to be associated with various factors in the univariable regression analyses, including age, sex, image quality, uncorrected visual acuity, intraocular pressure, spherical diopter, spherical equivalent, axial length, anterior chamber depth, and lens thickness. But, in multivariable regression, only sex (standardized $\beta = -17.26$, female vs. male), age ($\beta = -1.61$ per 1 year), and axial length ($\beta = -18.62$ per 1 mm) were statistically associated with the mean macular CT (Table) and were used in the analysis of the CT in each grid.

## CT Variation Related to Sex, Age, and Axial Length in 900 Grids

Compared to males, females exhibited thinner choroid in all 900 grids, ranging from 0.5 to 26.9 µm. The difference was minimal in the inferior nasal, superior nasal, and middle temporal regions but was more pronounced in the central regions (Fig. 2A). Both aging and axial length elongation were associated with choroid thinning in all 900 grids. For every 10-year increase in age, the decrease in CT ranged from 8.74 to 19.87 µm, which was more prominent in the temporal choroid than nasal (Fig. 2B). With a 1-mm increase in axial length, CT thinning ranged from 7.94 to 24.91 µm and was more prominent in subfoveal and nasal areas (Fig. 2C).

## Inter-Individual Variation in CT in the 900 Grids

Inter-individual variation of CT is reflected by the distribution of CoV, CoD, and CoVU. Figure 3A illustrates the inter-individual CoV of CT distribution, which ranged from 34.69% to 58.00% (mean 41.90% ± 5.28%) and increased from the temporal to the nasal. The CoD distribution pattern is shown in Figure 3B; values ranged from 18.41% to 39.66% and decreased from the temporal to nasal regions. Figure 3C shows a map of CoVU values (range, 23.05%–40.78%) to

**Table.** Univariable and Multivariable Regression Associations of Demographic and Ophthalmic Parameters With Mean Choroidal Thickness

| Parameter | | Univariable Regression | | Multivariable Regression | |
|---|---|---|---|---|---|
| | | $\beta$-Coefficient | *P* | $\beta$-Coefficient | *P* |
| Age (y), mean ± SD | 33.59 ± 25.21 | **−1.439** | **<0.001** | **−1.607** | **<0.001** |
| Female, *n* (%) | 212 (51.71) | **−23.634** | **0.001** | **−17.261** | **0.011** |
| Right eye, *n* (%) | 207 (50.49) | 10.639 | 0.127 | NI[a] | NI[a] |
| TopQ image quality, mean ± SD | 56.90 ± 9.12 | **1.823** | **<0.001** | −0.275 | 0.497 |
| Uncorrected visual acuity (logMAR), mean ± SD | 0.78 ± 0.39 | **−25.774** | **0.004** | −17.253 | 0.076 |
| Intraocular pressure (mmHg), mean ± SD | 15.36 ± 3.55 | **2.656** | **0.007** | 0.473 | 0.603 |
| Spherical diopter (D), mean ± SD | −1.96 ± 3.53 | **4.082** | **<0.001** | −3.647 | 0.519 |
| Cylindrical diopter (D), mean ± SD | −0.70 ± 1.29 | 0.202 | 0.074 | NI[a] | NI[a] |
| Axis of astigmatism, mean ± SD | 82.28 ± 70.47 | −0.025 | 0.620 | NI[a] | NI[a] |
| Spherical equivalent (D), mean ± SD | −2.31 ± 3.77 | **3.598** | **<0.001** | 1.72 | 0.745 |
| Axial length (mm), mean ± SD | 24.17 ± 1.47 | **−10.213** | **<0.001** | **−18.619** | **<0.001** |
| Anterior chamber depth (mm), mean ± SD | 3.46 ± 0.43 | **37.407** | **<0.001** | 16.533 | 0.154 |
| Lens thickness (mm), mean ± SD | 3.89 ± 0.55 | **−48.65** | **<0.001** | 8.925 | 0.515 |
| Central corneal thickness (µm), mean ± SD | 531.79 ± 33.30 | 0.079 | 0.499 | NI[a] | NI[a] |
| Mean choroidal thickness (µm), mean ± SD | 195.20 ± 70.53 | NI[a] | NI[a] | NI[a] | NI[a] |

Bold value means statistically significant ($P < 0.05$).
[a]Not included in the regression model.

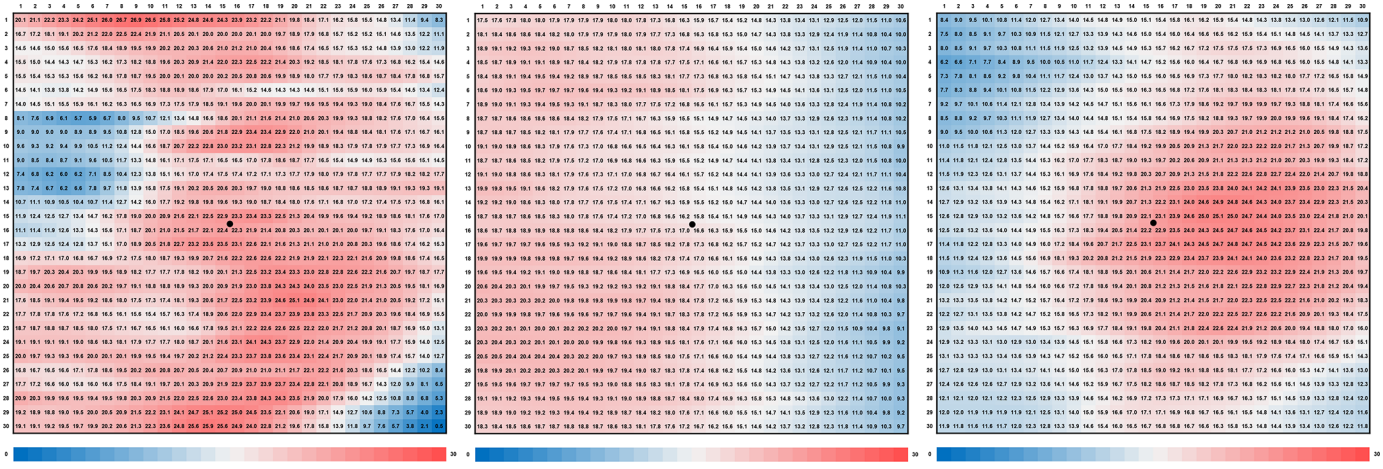

(A) (B) (C)

**Figure 2.** Topographic maps of CT attenuation with sex, age, and, axial length in 900 grids. (**A**) Differences in choroidal thickness between males and females. (**B**) Choroidal thickness thinning per 10 years of increasing age. (**C**) Choroidal thickness thinning per 1-mm increase in axial length. The left-to-right direction in all maps reflects temporal-to-nasal regions. The central *black dots* indicate the fovea. All numbers in the distribution maps are micrometers.

highlight the unexplained effect of factors other than sex, age, and axial length that were more pronounced in the nasal regions compared to the temporal region.

## Discussion

Our study has found that the thinning pattern of the choroid with aging is notably more pronounced in the temporal area, whereas it becomes more evident in the subfoveal and nasal areas with axial length elongation. Margolis and Spaide[19] observed a more pronounced decrease in CT with aging in normal eyes at positions 2.5 mm and 3.0 mm temporal to the fovea, but their investigation was limited to the CT on a horizontal line at 500-µm intervals crossing the fovea. Our map of thickness changes in the 900 grids effectively demonstrates that aging has more effect on the choroidal thinning process in the temporal area, which can be seen in samples 1 and 2 in Figure 4. Previ-

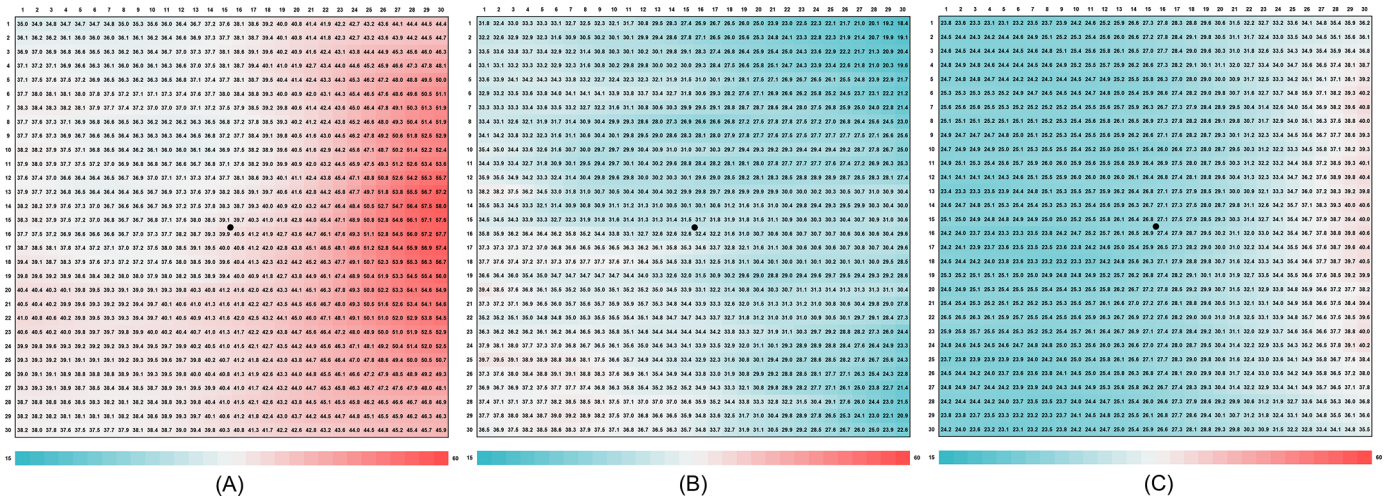


**Figure 3.** Topographic maps of inter-individual variation of macular CT. (**A**) Coefficient of variation. (**B**) Coefficient of determination, which represents the percentage of variation that can be explained by gender, age, and axial length. (**C**) Coefficient of variance unexplained, which represents the residual variation. The left-to-right direction in all maps reflects temporal-to-nasal areas around the fovea. The central *black dots* indicate the fovea. All numbers in the distribution maps are percentages.

ous studies have shown decreases in vascular density, overall luminal area, and choriocapillaris diameter with age,[25] whereas the temporal parafoveal and perifoveal areas exhibit higher choriocapillaris and choroidal vascular density.[26] Thus, the patterns of choroidal thinning associated with aging may be attributed to the greater impact of vascular density decreasing in the temporal regions.

Elongation of the axial length has a greater impact on the subfoveal and nasal areas, which are critical areas for ophthalmologists to evaluate to monitor the progression of myopia, particularly the development of myopic maculopathy. Deng et al.[27] reported that myopic individuals exhibit pronounced thinning of the choroid at the central foveal region, as well as in the temporal and inferior sectors of the peripapillary region, which can be explained by the uneven expansion of the posterior pole during the development of myopia. Fang et al.[28] demonstrated that, in eyes with myopia, choroidal thinning initially manifests as tessellation and subsequently progresses from the peripapillary to macular regions, resulting in diffused choroidal atrophy and the development of myopic maculopathy. Our choroidal changes map based on axial length elongation provides support for the observed choroidal thinning pattern in myopia eyes. Samples 1 and 3 in Figure 4 are vivid examples of the choroidal attenuation in the nasal region. The detailed distribution in the 900 grids provides us with a more intuitive way to monitor the progression of myopia, as compared to the sectors of the ETDRS and 3-mm areas toward the fovea.

Previous studies have found that the mean CT,[29] subfoveal CT,[10,30] and CT at 1 or 3 mm from the fovea[31] were significantly thicker in men compared to women. Our study initially found that in 900 subregions the CT values of males were consistently thicker than those of females, particularly in the subfoveal and inferior areas. Samples 1 and 4 in Figure 4 illustrate the difference in CT values between males and females. The variation in choroidal thickness between men and women may be explained by the elevated basal sympathetic tone in women,[25,32] which in turn may lead to relatively narrower choroidal blood vessels. Also, the difference in hormone levels may be another factor, given that women experience a significant decrease in choroidal thickness during the mid-luteal phase of the menstrual cycle.[25,29] In our study, the map of CT differences between males and females provides additional evidence of the physiological distinctions in different sexes, and this may explain the sex differences in the prevalence of some macular diseases. For example, central serous chorioretinopathy is more prevalent among males than females.[33]

To our knowledge, no comparable studies have been conducted that would provide a comparison for our results of the distributions of CoV, CoD, and CoVU for the choroid. The CoD map (Fig. 3B) showed greater CT variation attributable to sex, age, and axial length in the temporal region. Additionally, the CoV and CoVU maps indicate a substantial decrease from the temporal regions to the nasal regions, signifying that the inter-individual choroidal variation in the tempo-

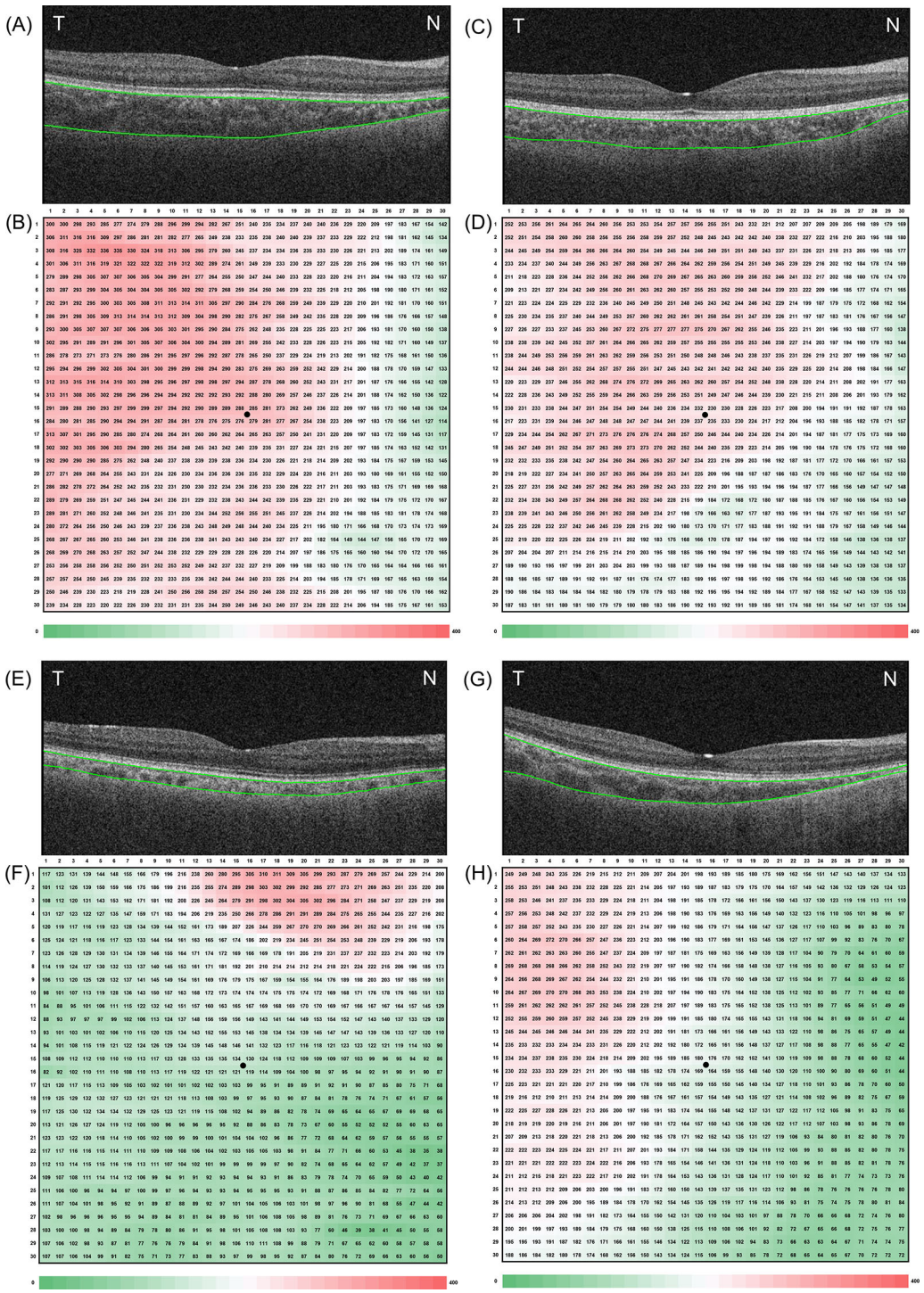


**Figure 4.** Examples of CT maps and B-scans of the fovea. (**A**, **B**) A 10-year-old male with an axial length of 23.08 mm. (**C**, **D**) A 73-year-old male with an axial length of 22.99 mm. (**E**, **F**) An 11-year-old male with an axial length of 26.13 mm. (**G**, **H**.) A 13-year-old female with an axial length of 22.84 mm.

ral area is less pronounced compared to the nasal region. This is the first attempt to describe the inter-individual CT variances within precise areas of 0.2 × 0.2 mm. Several studies that have also utilized the 900-grid algorithm to analyze CT distribution divided the macular region into five zones according to the CT in 900 grids but did not investigate the inter-individual variation.[20,21] Therefore, the potential mechanisms of inter-individual choroidal variation remain uncertain and deserve further exploration in the future.

We recognize that the current study had some limitations. First, the retrospective design might lead to biased results due to not considering choroidal diurnal variation or water intake. Second, all samples were obtained from eyes without macular disorders, and the changing pattern of CT in diseased eyes requires further investigation. Finally, the analysis was limited to the macular region of the choroid, but other areas of the fundus should also be investigated in future studies.

In conclusion, our study innovatively regarded each small choroidal subregion (0.2 × 0.2 mm) as an independent area to develop a precise topographic map for better understanding of the inter-individual choroidal variations in healthy eyes. Such an approach could be helpful for identifying the choroidal physiology and distinguishing pathological alterations from physiological variations.

## Acknowledgments

The authors express their sincere gratitude to everyone who contributed to the completion of this study. We are grateful to the JSIEC and staff members, who generously provided their time, knowledge, and resources for this study.

Supported by the Shantou Science and Technology Project (190917085269835) and a 2020 Li Ka Shing Foundation Cross-Disciplinary Research Grant (2020LKSFG14B). The sponsor or funding organization had no role in the design or conduct of this research.

Disclosure: **Z. Jiang**, None; **T. Lin**, None; **A. Lin**, None; **X. Liu**, None; **X. Mai**, None; **J. Lin**, None; **C.Y.L. Cheung**, None; **H. Chen**, None

## References

1. Sekiryu T. Choroidal imaging using optical coherence tomography: techniques and interpretations. *Jpn J Ophthalmol*. 2022;66:213–226.
2. Laviers H, Zambarakji H. Enhanced depth imaging-OCT of the choroid: a review of the current literature. *Graefes Arch Clin Exp Ophthalmol*. 2014;252:1871–1883.
3. Adhi M, Liu JJ, Qavi AH, et al. Choroidal analysis in healthy eyes using swept-source optical coherence tomography compared to spectral domain optical coherence tomography. *Am J Ophthalmol*. 2014;157:1272–1281.e1.
4. Fujiwara A, Shiragami C, Shirakata Y, Manabe S, Izumibata S, Shiraga F. Enhanced depth imaging spectral-domain optical coherence tomography of subfoveal choroidal thickness in normal Japanese eyes. *Jpn J Ophthalmol*. 2012;56:230–235.
5. Li XQ, Jeppesen P, Larsen M, Munch IC. Subfoveal choroidal thickness in 1323 children aged 11 to 12 years and association with puberty: the Copenhagen Child Cohort 2000 Eye Study. *Invest Ophthalmol Vis Sci*. 2014;55:550–555.
6. Nickla DL, Wallman J. The multifunctional choroid. *Prog Retin Eye Res*. 2010;29:144–168.
7. Chung SE, Kang SW, Lee JH, Kim YT. Choroidal thickness in polypoidal choroidal vasculopathy and exudative age-related macular degeneration. *Ophthalmology*. 2011;118:840–845.
8. Zhang JM, Wu JF, Chen JH, et al. Macular choroidal thickness in children: the Shandong children eye study. *Invest Ophthalmol Vis Sci*. 2015;56:7646–7652.
9. Borooah S, Sim PY, Phatak S, et al. Pachychoroid spectrum disease. *Acta Ophthalmol*. 2021;99:e806–e822.
10. Wei WB, Xu L, Jonas JB, et al. Subfoveal choroidal thickness: the Beijing eye study. *Ophthalmology*. 2013;120:175–180.
11. Barteselli G, Chhablani J, El-Emam S, et al. Choroidal volume variations with age, axial length, and sex in healthy subjects: a three-dimensional analysis. *Ophthalmology*. 2012;119:2572–2578.
12. Hirata M, Tsujikawa A, Matsumoto A, et al. Macular choroidal thickness and volume in normal subjects measured by swept-source optical coherence tomography. *Invest Ophthalmol Vis Sci*. 2011;52:4971–4978.
13. Rong Y, Jiang Z, Wu W, et al. Direct estimation of choroidal thickness in optical coherence tomography images with convolutional neural networks. *J Clin Med*. 2022;11:3203.
14. Touhami S, Philippakis E, Mrejen S, et al. Topographic variations of choroidal thickness in healthy eyes on swept-source optical coherence tomography. *Invest Ophthalmol Vis Sci*. 2020;61:38.
15. Gao J, Rao CH, Li F, Liu L, Liu KJ. Ultra-widefield swept-source optical coherence tomography angiography in the assessment of choroidal changes in young adults with myopia. *Transl Vis Sci Technol*. 2022;11:14.
16. Hirano M, Muraoka Y, Kogo T, et al. Analysis of widefield choroidal thickness maps of healthy eyes using swept source optical coherence tomography. *Sci Rep*. 2023;13:11904.

17. Ikuno Y, Kawaguchi K, Nouchi T, Yasuno Y. Choroidal thickness in healthy Japanese subjects. *Invest Ophthalmol Vis Sci*. 2010;51:2173–2176.
18. He X, Jin P, Zou H, et al. Choroidal thickness in healthy Chinese children aged 6 to 12: the Shanghai children eye study. *Retina*. 2017;37:368–375.
19. Margolis R, Spaide RF. A pilot study of enhanced depth imaging optical coherence tomography of the choroid in normal eyes. *Am J Ophthalmol*. 2009;147:811–815.
20. Bartol-Puyal FA, Isanta C, Ruiz-Moreno Ó, Abadia B, Calvo P, Pablo L. Distribution of choroidal thinning in high myopia, diabetes mellitus, and aging: a swept-source OCT study. *J Ophthalmol*. 2019;2019:3567813.
21. Abadia B, Bartol-Puyal FA, Calvo P, Verdes G, Isanta C, Pablo LE. Mapping choroidal thickness in patients with type 2 diabetes. *Can J Ophthalmol*. 2020;55:45–51.
22. Chen FK, Yeoh J, Rahman W, Patel PJ, Tufail A, DaCruz L. Topographic variation and interocular symmetry of macular choroidal thickness using enhanced depth imaging optical coherence tomography. *Invest Ophthalmol Vis Sci*. 2012;53:975–985.
23. Kim MS, Lim HB, Lee WH, Kim K-M, Nam KY, Kim J-Y. Wide-field swept-source optical coherence tomography analysis of interocular symmetry of choroidal thickness in healthy young individuals. *Invest Ophthalmol Vis Sci*. 2021;62:5.
24. Deng J, Jin J, Zhang B, et al. Effect of ocular magnification on macular choroidal thickness measurements made using optical coherence tomography in children. *Curr Eye Res*. 2022;47:1538–1546.
25. Tan KA, Gupta P, Agarwal A, et al. State of science: choroidal thickness and systemic health. *Surv Ophthalmol*. 2016;61:566–581.
26. Lal B, Alonso-Caneiro D, Read SA, Carkeet A. Diurnal changes in choroidal optical coherence tomography angiography indices over 24 hours in healthy young adults. *Sci Rep*. 2023;13:3551.
27. Deng J, Li X, Jin J, et al. Distribution pattern of choroidal thickness at the posterior pole in Chinese children with myopia. *Invest Ophthalmol Vis Sci*. 2018;59:1577–1586.
28. Fang Y, Du R, Nagaoka N, et al. OCT-based diagnostic criteria for different stages of myopic maculopathy. *Ophthalmology*. 2019;126:1018–1032.
29. Ooto S, Hangai M, Yoshimura N. Effects of sex and age on the normal retinal and choroidal structures on optical coherence tomography. *Curr Eye Res*. 2015;40:213–225.
30. Li XQ, Larsen M, Munch IC. Subfoveal choroidal thickness in relation to sex and axial length in 93 Danish university students. *Invest Ophthalmol Vis Sci*. 2011;52:8438–8441.
31. Zeng J, Liu R, Zhang X-Y, et al. [Relationship between gender and posterior pole choroidal thickness in normal eyes]. *Zhonghua yan ke za zhi*. 2012;48:1093–1096.
32. Cooke JP, Creager MA, Osmundson PJ, Shepherd JT. Sex differences in control of cutaneous blood flow. *Circulation*. 1990;82:1607–1615.
33. Yang L, Jonas JB, Wei W. Optical coherence tomography-assisted enhanced depth imaging of central serous chorioretinopathy. *Invest Ophthalmol Vis Sci*. 2013;54:4659–4665.